^{8}Be + ^{8}Be and ^{12}C + α breakup states in ^{16}O populated via the ^{13}C(^{4}He,4α)n reaction

N. Curtis,[1,*] S. Almaraz-Calderon,[2] A. Aprahamian,[2] N. I. Ashwood,[1] M. Barr,[1] B. Bucher,[2] P. Copp,[3] M. Couder,[2] X. Fang,[2] M. Freer,[1] G. Goldring,[4] F. Jung,[2] S. R. Lesher,[3] W. Lu,[2] J. D. Malcolm,[1] A. Roberts,[2] W. P. Tan,[2] C. Wheldon,[1] and V. A. Ziman[1]

[1]*School of Physics and Astronomy, University of Birmingham, Edgbaston, Birmingham B15 2TT, United Kingdom*

[2]*Institute for Structure and Nuclear Astrophysics, Department of Physics, University of Notre Dame, Notre Dame, Indiana 46556, USA*

[3]*Department of Physics, University of Wisconsin-La Crosse, La Crosse, Wisconsin 54601, USA*

[4]*Department of Particle Physics, Weizmann Institute, 76100 Rehovot, Israel*

(Received 12 June 2015; revised manuscript received 21 July 2016; published 13 September 2016)

The ^{13}C(^{4}He,4α)n breakup reaction has been studied at beam energies of 27.0, 27.5, and 28.0 MeV. A comparison with previous measurements of the ^{12}C(^{4}He,^{8}Be)^{8}Be excitation function and ^{12}C(^{16}O,4α)^{12}C breakup channel suggests the ^{8}Be$_{gs}$ + ^{8}Be$_{gs}$ decay of ^{16}O is observed from a possible 2^+ state at 17.3 ± 0.2 MeV, a 4^+ state at 18.0 ± 0.2 MeV, a 2^+ or 4^+ state at 19.4 ± 0.2 MeV, and a 4^+ or 6^+ state at 21.0 ± 0.2 MeV. The 2^+ or 4^+ assignment for the (19.4 ± 0.2)-MeV state appears to be supported by the relative cross sections expected for resonant and sequential breakup reactions.

DOI: 10.1103/PhysRevC.94.034313

I. INTRODUCTION

For nearly 50 years it has been believed that a 4α linear chain state exists in ^{16}O, following the observation of a highly deformed rotational band in the ^{8}Be + ^{8}Be decay of this nucleus. A measurement of the ^{12}C(^{4}He,^{8}Be)^{8}Be excitation function by Chevallier *et al.* [1] indicated that a series of 2^+ to 6^+ resonances were populated in the 16–21 MeV excitation energy (E_x) range. The energy-spin systematics suggested a highly deformed rotational band was being populated, the moment of inertia of which was approximately four times greater than that calculated classically for the spherical ^{16}O ground state. The conclusion of Chevallier *et al.* [1] was that the structure, if confirmed, corresponds to a linear chain state of four α particles, arranged in a rigidly rotating body.

Such a configuration had previously been predicted to exist by Morinaga [2], who suggested that the 6.049-MeV 0^+ and 6.917-MeV 2^+ states in ^{16}O form a rotational band, the moment of inertia of which is consistent with four α particles touching in a row. However, the 0^+ member of this band, the state at 6.049 MeV, is almost 11 MeV lower in excitation than the 16.7 MeV bandhead energy of the Chevallier rotational band, and it is now well established [3] that both states are actually members of the $K^\pi = 0^+$ 4p-4h rotational band in ^{16}O. This band has additional 4^+ and 6^+ members at 10.356 and 16.275 MeV, respectively, and is believed to possess an α + ^{12}C structure (see, for example, Refs. [4–9]) with the 4^+ and 2^+ [10] and 2^+ and 0^+ [11] states being connected by strong $E2$ transitions, indicative of the rotational structure.

Later studies of the ^{12}C(^{4}He,^{8}Be)^{8}Be [12–14] and ^{12}C(^{4}He,^{12}C* [7.65 MeV, 0^+_2])α [15] reactions failed to find evidence for the 8^+ member of the proposed [1] linear chain state rotational band. This, based on the energy-spin systematics of the Chevallier resonances, should appear at an excitation energy of ∼21.3 MeV. Tentative evidence for an 8^+ state was reported at E_x(^{16}O) = 22.5 ± 0.5 MeV by Sanders *et al.* [16], following a study of the ^{12}C(^{12}C,^{8}Be)^{16}O*, ^{16}O$^* \rightarrow \alpha + {}^{12}C_{gs}$ reaction, although this state was thought to be a member of the $K^\pi = 0^+$ 4p-4h band (built on the 6.049 MeV, 0^+ state) in ^{16}O, rather than the chain state band. The 8^+ spin assignment for the state was later questioned [17], however, and no longer appears in the ^{16}O compilation [3].

A study of the ^{12}C(^{16}O,4α)^{12}C breakup reaction by Freer *et al.* [18] also provided evidence for a rotational band in the same E_x region as the Chevallier work. Several of the observed breakup states appear to correspond to resonances observed by Chevallier *et al.* [1], but others do not, and although the bandhead energy (E_0) of 17.0 ± 0.7 MeV is consistent with the Chevallier value of 16.7 MeV, the rotational parameter ($\hbar^2/2I$, where I is the moment of inertia) of 95 ± 20 keV is somewhat larger than the 64 keV seen in Ref. [1]. It is not clear, therefore, if the same or different structures are being populated by the two different reaction mechanisms. A number of states in the E_x(^{16}O) = 17.7–35.1 MeV and 6^+ to 10^+ angular momentum range have also been seen in the ^{12}C(^{12}C,^{8}Be ^{8}Be)^{8}Be reaction [19]. However, whereas the states observed below 25 MeV appear to lie on same band as those of Chevallier *et al.* [1], those above this energy do not, and it is not clear if more than one rotational band is being populated in the reaction.

The ^{12}C(^{4}He,^{8}Be)^{8}Be excitation function has become the focus of attention again in recent years, with two new repeat measurements of the earlier Chevallier *et al.* [1] work. The results of Soylu *et al.* [20] show some agreement with the Chevallier data, although different ^{8}Be center of mass angular ranges were covered in the two experiments. The latest study [21] of this reaction does show good agreement with the excitation functions of both Chevallier *et al.* [1] and Brochard *et al.* [14], but distinct discrepancies do arise between the spin assignments made for the resonances in the different measurements. This brings into question the existence of a linear chain state of four α particles in ^{16}O.

*Corresponding author: n.curtis@bham.ac.uk

The theoretical picture is also somewhat unclear. The rotational band proposed by Chevallier *et al.* [1] is supported by the alpha cluster model (ACM) calculations of Bauhoff *et al.* [5]. In this study a chain state of four α particles was found, with the same rotational parameter, and similar bandhead energy (16.3 MeV), as the Chevallier *et al.* [1] band. A slightly higher bandhead energy of 18.9 MeV, and a band termination of $L_{\max} = 21\hbar$, was found in the cranked Bloch-Brink cluster model calculations of Merchant and Rae [22,23]. These same authors also used a coupled channels approach, and a $^{8}\mathrm{Be} + {}^{8}\mathrm{Be}$ description of ^{16}O [24]. Although no 0^+ cluster states were found in these calculations, 2^+ to 16^+ resonances were. These lie on a rotational band with $\hbar^2/2I = 100$ keV, in excellent agreement with the band observed by Freer *et al.* [18] (although the experimental bandhead lies 5 MeV lower than the model would suggest).

However, more recent Skyrme cranked Hartree-Fock calculations by Ichikawa *et al.* [25] suggest that a linear α chain will only be stable in the (13–18)$\hbar$ angular momentum region. Although the (60–80 keV) rotational parameter obtained for the four α chains agrees with both the Chevallier *et al.* [1] measurement and the Bauhoff *et al.* [5] ACM calculation, the bandhead is found to be in the region of $E_{\mathrm{x}} = 38$ MeV, significantly higher than the 16–17 MeV range of Refs. [1,5]. A similar bandhead energy of ∼37 MeV was also found in the covariant density functional theory (CDFT) work of Lang and Peng-Wei [26]. The CDFT approach was also used by Yao *et al.* [27] to study both low-spin (using the generator coordinate method) and high-spin (using a cranked relativistic mean-field approach) states in ^{16}O. An α-chain state structure was found in both spin regions, with $\hbar^2/2I$ and E_0 being 123 keV and 29.6 MeV in the low-spin (0 $\hbar$–6 $\hbar$), and 110 keV and 30.2 MeV in the high-spin (12.6 $\hbar$–18.0$\hbar$) calculations, respectively. The average rotational parameter for the two spin regions is a factor of ∼1.8 larger than the Chevallier *et al.* [1] and Bauhoff *et al.* [5] values, although only a factor of ∼1.2 greater than the measurement obtained by Freer *et al.* [18]. The bandhead energies are quite different, however.

Perhaps the most intriguing recent theoretical predictions for the excitation energy region above 15 MeV in ^{16}O concern α-condensate states [28]. Ohkubo and Hirabayashi [29] used a double folding model and the coupled channels method to study the proposed α-chain state in ^{16}O. The calculations suggest that the α-chain state should have an $\alpha + {}^{12}\mathrm{C}^*$ [7.65 MeV, 0_2^+] structure, where the three α particles in the $^{12}\mathrm{C}^*$ [7.65 MeV, 0_2^+] Hoyle state are condensed. The bandhead, suggested to be a superfluid of four α particles, is found to be the 0^+ state at 15.1 MeV. Suhara *et al.* [30] reached a similar conclusion, following generator coordinate method calculations using a sum of a large number of Brink wave functions. The results show an extremely large overlap with a single Tohsaki-Horiuchi-Schuck-Röpke [28] condensate wave function, suggesting the states studied in ^{16}O are "gaslike." It it proposed that the α-linear chain state in ^{16}O has a one-dimensional α-condensate character, with the four α particles trapped in a one-dimensional potential in a nonlocalized manner, like a "gas."

The status of the four α-linear chain states in ^{16}O clearly remains uncertain at present, with neither experiment nor theory providing a particularly consistent picture of the energy-spin regime of the proposed rotational band. In an effort to improve the understanding of the 16–22 MeV excitation energy region in ^{16}O, a measurement of the $^{13}\mathrm{C}(^{4}\mathrm{He},{}^{8}\mathrm{Be}\ {}^{8}\mathrm{Be})n$ and $^{13}\mathrm{C}(^{4}\mathrm{He},{}^{12}\mathrm{C}^*\ \alpha)n$, ${}^{12}\mathrm{C}^* \rightarrow {}^{8}\mathrm{Be} + \alpha$ breakup reactions was performed. It was hoped that, by studying a different reaction mechanism than the $^{12}\mathrm{C}(^{4}\mathrm{He},{}^{8}\mathrm{Be})^{8}\mathrm{Be}$ excitation function measurements of Refs. [1,12–14,20,21] and the breakup work of Refs. [18,19], fresh insights into the nature of the states in ^{16}O in this excitation energy region would be obtained.

II. EXPERIMENTAL DETAILS

The experiment was performed at the University of Notre Dame FN Tandem facility. A ^{4}He beam was used at energies of 27.0, 27.5, and 28.0 MeV, with beam exposures of 48, 100, and 174 μC, respectively. Data were also taken at 22.0 MeV (with a beam exposure of 278 μC), but the yield and coverage were found to be minimal in the analysis, and the results are not presented. The beam was used to bombard a self-supporting ^{13}C target of 45 $\mu\mathrm{g/cm}^2$ nominal thickness, made from carbon material enriched to a quoted value of 99% ^{13}C. The $^{13}\mathrm{C}(^{4}\mathrm{He},{}^{8}\mathrm{Be}\ {}^{8}\mathrm{Be})n$ and $^{13}\mathrm{C}(^{4}\mathrm{He},{}^{12}\mathrm{C}^*\ \alpha)n$, ${}^{12}\mathrm{C}^* \rightarrow {}^{8}\mathrm{Be} + \alpha$ reactions of interest both have a final state of four α particles and a neutron, as the ^{8}Be ground state is unbound to $\alpha + \alpha$ decay by 92 keV. An array of four double sided silicon strip detectors (DSSDs) was employed in order to detect the four α particles. Each DSSD was 500 μm thick and 5×5 cm^2 in active area. Each face was segmented into 16 strips of 3 mm width, with the front face strips being horizontal and those on the rear face vertical. All four detectors were centered on the beam axis vertically, with two DSSDs being placed on either side of the beam. The detector distances and center angles were 10.0 cm and $+50.8^\circ$, 14.0 cm and $+23.5^\circ$, 13.9 cm and -28.6°, and 10.7 cm and -54.5°. The detector energy calibrations were performed using elastic scattering of a ^{4}He beam from Pb, Al, and C targets and a mixed (^{148}Gd and ^{241}Am) α source. The detector energy resolution, as measured with the mixed α source, was ∼80 keV.

III. ANALYSIS AND RESULTS

After selecting events in which four particles were detected in the DSSD array, energy and position calibrations were applied to the data. As no particle identification was provided directly by the detectors, the four hits were assumed to be α particles in the analysis. The $^{13}\mathrm{C}(^{4}\mathrm{He},{}^{8}\mathrm{Be}\ {}^{8}\mathrm{Be})n$ and $^{13}\mathrm{C}(^{4}\mathrm{He},{}^{12}\mathrm{C}^*\ \alpha)n$ channels were identified using a Q-value spectrum produced by summing the energy of the four detected α particles (E_1 to E_4) with that of the undetected neutron (E_n). The total energy in the exit channel, $E_{\mathrm{tot}} = E_1 + E_2 + E_3 + E_4 + E_n$, is equal to the sum of the beam energy and the Q value for the reaction, $E_{\mathrm{tot}} = E_{\mathrm{beam}} + Q$ [31]. As the two ^{16}O decay channels of interest ($^{8}\mathrm{Be} + {}^{8}\mathrm{Be}$ and $^{12}\mathrm{C}^* + \alpha$) share the same final state of $4\alpha + n$, the reaction Q value is the same for both: $Q = -12.22$ MeV. The undetected neutron energy was determined for each event from the missing momentum between the beam and four detected α particles, $\mathbf{p}_n = \mathbf{p}_{\mathrm{beam}} - \mathbf{p}_1 - \mathbf{p}_2 - \mathbf{p}_3 - \mathbf{p}_4$, and by making the

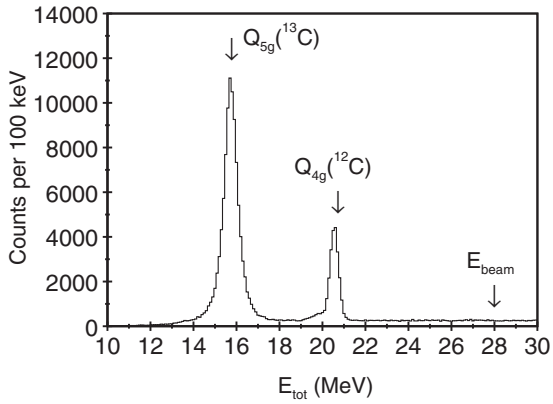

FIG. 1. Total energy spectrum at a beam energy of 28.0 MeV. The expected positions of peaks corresponding to the ^{13}C(^{4}He,$\alpha\alpha\alpha$)n and ^{12}C(^{4}He,$\alpha\alpha\alpha$)α reactions are labeled as Q_{5g}(^{13}C) and Q_{4g}(^{12}C), respectively.

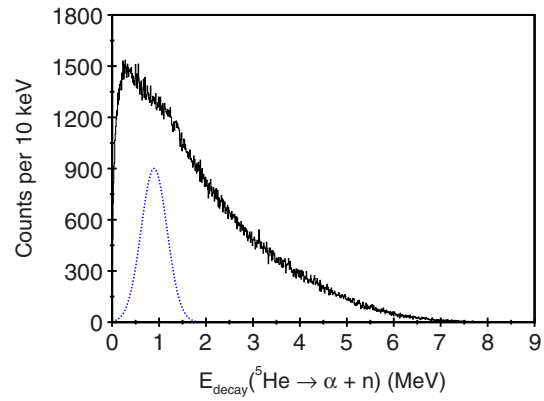

FIG. 2. Decay energy for ^{5}He $\rightarrow \alpha + n$ at a beam energy of 28.0 MeV. The (blue) dotted Gaussian line shape indicates the expected position (0.894 MeV) and full width at half maximum (FWHM) (0.648 MeV) of the ^{5}He ground state.

assumption that the missing mass was that of a neutron. Any misidentification of a detected particle (the particle is not an α particle as assumed) will lead to an incorrect momentum calculation for that particle, and an incorrectly assumed recoil mass. For such events the calculated $E_{\rm tot}$ energy will be incorrect, and hence these events will not appear at the energy of the reaction channels of interest, $E_{\rm tot} = E_{\rm beam} + Q$.

In Fig. 1 the $E_{\rm tot}$ spectrum obtained at a beam energy of 28.0 MeV is shown. The strong peak at $E_{\rm tot} =$ 15.74 MeV, labeled Q_{5g}(^{13}C), corresponds to the ^{13}C(^{4}He,4α)n channel of interest, with all five final state particles being emitted in the ground state. For this reaction $Q = -12.22$ MeV, and hence the predicted position of the Q_{5g}(^{13}C) peak is $28.0 - 12.22 = 15.78$ MeV. The additional peak in Fig. 1, labeled Q_{4g}(^{12}C), corresponds to the ^{12}C(^{4}He,4α) channel, for which $Q =$ -7.28 MeV. The predicted energy for this peak is $28.0 - 7.28 = 20.72$ MeV, and the measured value 20.55 MeV. The background below the two peaks (extending to the beam energy and higher) corresponds to events where one (or more) of the detected particles has been misidentified.

After selecting events within the Q_{5g}(^{13}C) peak seen in Fig. 1, a search was made for the decay of ^{5}He $\rightarrow \alpha + n$. This was performed to ensure background events were not being detected from the (a) ^{13}C(^{4}He,^{12}C*)^{5}He, ^{12}C* $\rightarrow$ ^{8}Be + α, (b) ^{13}C(^{4}He,^{9}Be*)^{8}Be, ^{9}Be* $\rightarrow$ ^{5}He + α, (c) ^{13}C(^{4}He,^{13}C*)α, ^{13}C* $\rightarrow$ ^{8}Be + ^{5}He, or (d) ^{13}C(^{4}He,^{13}C*)α, ^{13}C* $\rightarrow$ ^{9}Be* + α, ^{9}Be* $\rightarrow$ ^{5}He + α channels, none of which proceeds via the ^{16}O nucleus of interest.

The decay energy for any n-body decay of a parent nucleus may be determined from the kinetic energies and momenta of the decay particles:

$$\mathbf{P}_{\rm parent} = \sum_{i=1}^{n} \mathbf{P}_{{\rm particle}_i}, \quad E_{\rm parent} = \mathbf{P}^2_{\rm parent}/2m_{\rm parent},$$

where $m_{\rm parent}$ is the mass of the decaying parent nucleus, and

$$E_{\rm decay} = \left(\sum_{i=1}^{n} E_{{\rm particle}_i}\right) - E_{\rm parent}.$$

The decay energy is related to the excitation energy ($E_{\rm x}$) of the decaying nucleus via $E_{\rm x} = E_{\rm decay} - Q_n$, where Q_n is the n-body decay Q value.

The decay energy spectrum for the $\alpha + n$ decay of ^{5}He, obtained at a beam energy of 28.0 MeV, is shown in Fig. 2 (for all four combinations of $\alpha + n$ together). The expected position (0.894 MeV) and width (FWHM = 0.648 MeV) of the ^{5}He ground state is indicated by the (blue) dotted line. There is no compelling evidence for such a peak, thus ruling out significant background from the four channels, (a)–(d), involving ^{5}He decay mentioned above.

The decay energy spectrum for the $\alpha + \alpha$ decay of ^{8}Be is shown in Fig. 3. This was obtained at a beam energy of 28.0 MeV and includes all three possible paired combinations of the four α particles together. For each event the three possible pairs of combinations are (1) $\alpha_1 + \alpha_2$ and $\alpha_3 + \alpha_4$, (2) $\alpha_1 + \alpha_3$ and $\alpha_2 + \alpha_4$, and (3) $\alpha_1 + \alpha_4$ and $\alpha_2 + \alpha_3$. The strong peak observed at $E_{\rm decay} = 92$ keV corresponds to decay from the ^{8}Be ground state (^{8}Be$_{\rm gs}$). To select events arising from the ^{8}Be$_{\rm gs}$ + ^{8}Be$_{\rm gs}$ decay of ^{16}O, a search was made for events in which the ^{8}Be decay energy of both pairs of

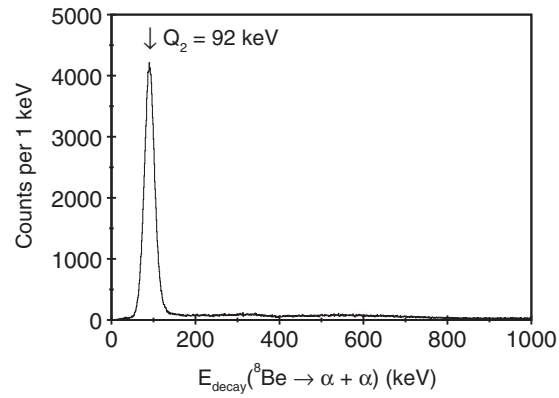

FIG. 3. Decay energy for ^{8}Be $\rightarrow \alpha + \alpha$ at a beam energy of 28.0 MeV. The arrow indicates the known ^{8}Be ground state energy (92 keV).

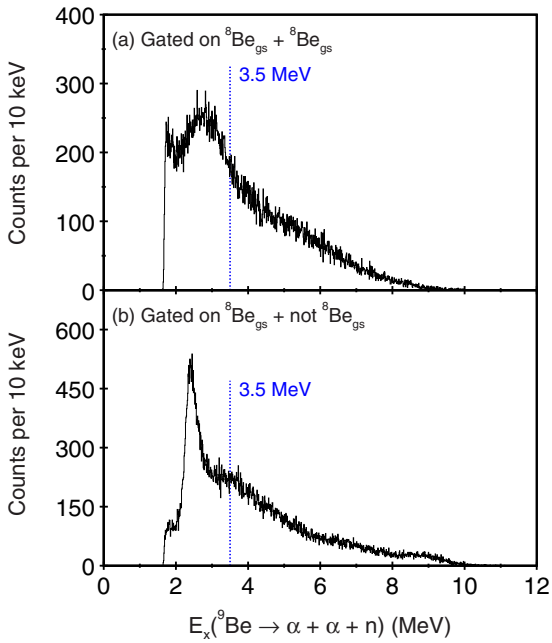

FIG. 4. Excitation energy for $^{9}\mathrm{Be} \rightarrow \alpha + \alpha + n$ at a beam energy of 28.0 MeV. The data are gated on (a) two ^{8}Be ground state pairs and (b) one ^{8}Be ground state pair and one pair not in the ^{8}Be ground state. The (blue) dotted vertical line indicates the energy of the 3.5-MeV gate applied to the data (see text).

one of the possible $\alpha + \alpha$ combinations (1 to 3, as noted above) lay within the peak, whereas the other four α pairs, corresponding to the other two combinations, did not. Such events are denoted "$^{8}\mathrm{Be}_{gs} + {}^{8}\mathrm{Be}_{gs}$." Similarly, in order to select the $^{12}\mathrm{C}^{*} + \alpha$, $^{12}\mathrm{C}^{*} \rightarrow {}^{8}\mathrm{Be} + \alpha$ decay of ^{16}O, events were selected in which only one of the six possible α pairs lay within the ^{8}Be ground state peak observed in Fig. 3. These events are denoted "$^{8}\mathrm{Be}_{gs}$ + not $^{8}\mathrm{Be}_{gs}$."

Once events were selected as either (a) $^{8}\mathrm{Be}_{gs} + {}^{8}\mathrm{Be}_{gs}$ or (b) $^{8}\mathrm{Be}_{gs}$ + not $^{8}\mathrm{Be}_{gs}$, the two pairs of α particles were each used in conjunction with the reconstructed neutron to calculate the excitation energy for $^{9}\mathrm{Be} \rightarrow \alpha + \alpha + n$ [to give $E_x(^{9}\mathrm{Be}_1)$ and $E_x(^{9}\mathrm{Be}_2)$]. The resulting excitation energy spectra for (a) $^{8}\mathrm{Be}_{gs} + {}^{8}\mathrm{Be}_{gs}$ and (b) $^{8}\mathrm{Be}_{gs}$ + not $^{8}\mathrm{Be}_{gs}$ are shown in Fig. 4, for the data obtained at a beam energy of 28.0 MeV. In each case both $E_x(^{9}\mathrm{Be}_1)$ and $E_x(^{9}\mathrm{Be}_2)$ are plotted added together. In Fig. 4(a) a broad peak may be seen at $E_x(^{9}\mathrm{Be}) = 2.88$ MeV, which corresponds to the known 1080 ± 110 keV wide $\frac{1}{2}^{-}$ state at 2.78 MeV in ^{9}Be [32]. This state is populated in the $^{13}\mathrm{C}(^{4}\mathrm{He},{}^{9}\mathrm{Be}^{*})^{8}\mathrm{Be}_{gs}$, $^{9}\mathrm{Be}^{*} \rightarrow {}^{8}\mathrm{Be}_{gs} + n$ reaction, which does not proceed via the ^{16}O nucleus of interest. The $E_x(^{9}\mathrm{Be})$ experimental resolution at this energy is 400 keV. This value was obtained from a Monte Carlo simulation of the $^{13}\mathrm{C}(^{4}\mathrm{He},{}^{9}\mathrm{Be}^{*})^{8}\mathrm{Be}_{gs}$, $^{9}\mathrm{Be}^{*} \rightarrow {}^{8}\mathrm{Be}_{gs} + n$ reaction, which included the reaction kinematics, the detector acceptances, and the physical effects that contribute to the resolution (beam quality, beam and fragment energy loss, energy straggle and angular straggle in the target, and detector energy and position resolution). Adding the width of the state in quadrature to the experimental resolution suggests this state should be observed with an experimental width of ∼1150 keV, in excellent agreement with the 1140 ± 75 keV obtained by fitting a Gaussian peak above a smoothly varying background to the spectrum shown in Fig. 4(a). A clear peak may also be seen in Fig. 4(b), at an energy of $E_x(^{9}\mathrm{Be}) = 2.44$ MeV. This corresponds to the known ^{9}Be $\frac{5}{2}^{-}$ state at 2.43 MeV. This state arises from the population of the (a) $^{13}\mathrm{C}(^{4}\mathrm{He},{}^{9}\mathrm{Be}^{*})^{8}\mathrm{Be}^{*}$, $^{9}\mathrm{Be}^{*} \rightarrow {}^{8}\mathrm{Be}_{gs} + n$, (b) $^{13}\mathrm{C}(^{4}\mathrm{He},{}^{9}\mathrm{Be}^{*})^{8}\mathrm{Be}_{gs}$, $^{9}\mathrm{Be}^{*} \rightarrow {}^{8}\mathrm{Be}^{*} + n$, or (c) $^{13}\mathrm{C}(^{4}\mathrm{He},{}^{13}\mathrm{C}^{*})\alpha$, $^{13}\mathrm{C}^{*} \rightarrow {}^{9}\mathrm{Be}^{*} + \alpha$, $^{9}\mathrm{Be}^{*} \rightarrow {}^{8}\mathrm{Be}_{gs} + n$ channels, none of which decays via the ^{16}O nucleus of interest. The 2.43-MeV state in ^{9}Be has a width of only 0.78 keV [32], and hence the width of the observed peak, 370 ± 8 keV, is determined by the experimental resolution. The Monte Carlo simulation indicates this is 365 keV, in excellent agreement. To remove events from the ^{9}Be 2.78-MeV state [in the case of the $^{8}\mathrm{Be}_{gs} + {}^{8}\mathrm{Be}_{gs}$ events seen in Fig. 4(a)] and the 2.43-MeV state [for the $^{8}\mathrm{Be}_{gs}$ + not $^{8}\mathrm{Be}_{gs}$ events seen in Fig. 4(b)] a gate was applied to the data such that only events with $E_x(^{9}\mathrm{Be}) \geqslant 3.5$ MeV [indicated by the vertical (blue) dotted line in Fig. 4] are accepted. For consistency the same gate was applied to both the $^{8}\mathrm{Be}_{gs} + {}^{8}\mathrm{Be}_{gs}$ and the $^{8}\mathrm{Be}_{gs}$ + not $^{8}\mathrm{Be}_{gs}$ events.

A. The ^{8}Be + ^{8}Be decay of ^{16}O

The excitation energy spectra for the $^{8}\mathrm{Be}_{gs} + {}^{8}\mathrm{Be}_{gs}$ decay of ^{16}O, obtained from the $^{13}\mathrm{C}(^{4}\mathrm{He},{}^{8}\mathrm{Be}_{gs}\ {}^{8}\mathrm{Be}_{gs})n$ reaction (for all three beam energies added together) are shown in Fig. 5. In Fig. 5(a) all $^{8}\mathrm{Be}_{gs} + {}^{8}\mathrm{Be}_{gs}$ events are shown, whereas in Figs. 5(b) and 5(c) only those events for which $E_x(^{9}\mathrm{Be}) \geqslant 3.5$ MeV are displayed (see above). In both Figs. 5(a) and 5(b), the (blue) dot-dashed line indicates the experimental detection efficiency, at the central beam energy of 27.5 MeV. This was obtained from a Monte Carlo simulation of the reaction, in which the angular distributions, for both the production and subsequent decay of the excited ^{16}O, were isotropic. The peak efficiency values are noted in each case. The effect of the $E_x(^{9}\mathrm{Be}) \geqslant 3.5$ MeV gate, to significantly reduce the background in the $E_x(^{16}\mathrm{O}) = 20$–$24$ MeV region, can be seen by comparing Figs. 5(a) and 5(b).

In breakup reactions such as those studied here, it is usually possible to obtain spin information by studying the decaying fragment angular correlations [33]. In the case of the present $^{13}\mathrm{C}(^{4}\mathrm{He},{}^{8}\mathrm{Be}_{gs}\ {}^{8}\mathrm{Be}_{gs})n$ reaction, however, the angular correlations produced are featureless and simply reproduce the predicted coverage obtained from Monte Carlo simulations of the experiment. As such they are not shown, and it has not been possible to determine the spins of the states observed in Fig. 5.

B. The $^{12}\mathrm{C} + \alpha$ decay of ^{16}O

The $^{8}\mathrm{Be}_{gs}$ + not $^{8}\mathrm{Be}_{gs}$ events in the data have been assumed to arise from the $^{13}\mathrm{C}(^{4}\mathrm{He},{}^{16}\mathrm{O}^{*})n$, $^{16}\mathrm{O}^{*} \rightarrow {}^{12}\mathrm{C}^{*} + \alpha$, $^{12}\mathrm{C}^{*} \rightarrow {}^{8}\mathrm{Be}_{gs} + \alpha$, $^{8}\mathrm{Be}_{gs} \rightarrow \alpha + \alpha$ reaction. If the two α particles produced in the decay of the ^{8}Be ground state are labeled α_1 and α_2, then the two remaining α particles (α_3 and α_4) must arise from the $^{16}\mathrm{O}^{*} \rightarrow {}^{12}\mathrm{C}^{*} + \alpha$ and $^{12}\mathrm{C}^{*} \rightarrow {}^{8}\mathrm{Be}_{gs} + \alpha$ decays. As it is not possible to distinguish which α particle (α_3 or α_4) belongs to which decay, it is necessary to reconstruct

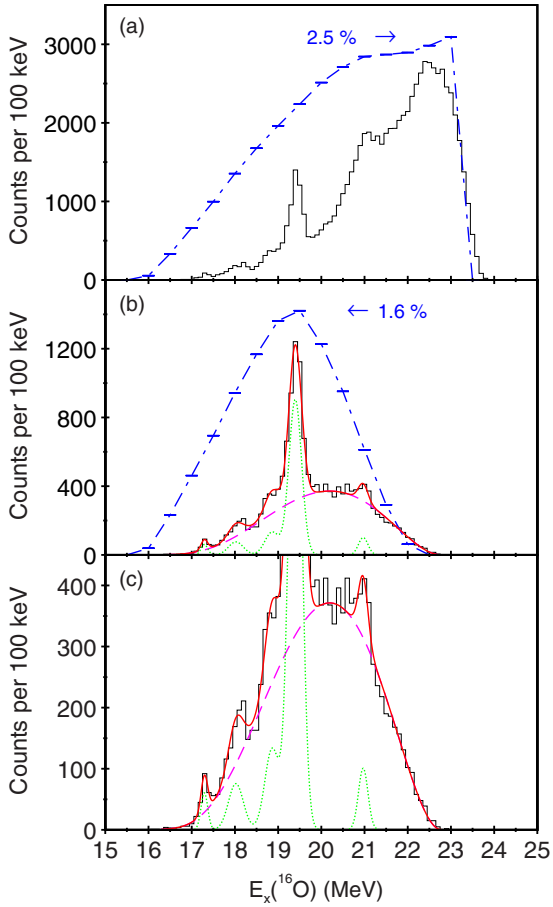

FIG. 5. Excitation energy for the $^{8}\mathrm{Be}_{gs} + {}^{8}\mathrm{Be}_{gs}$ decay of ^{16}O from (a) all events in the present data and (b, c) events with $E_x(^{9}\mathrm{Be}) \geqslant 3.5$ MeV. The (blue) dot-dashed lines represent the detection efficiency profiles, for which the peak values are given. (b, c) The results of a Gaussian peak fit are shown (see text).

the decaying ^{12}C nucleus in two ways, to give $E_x(^{12}\mathrm{C}^* \rightarrow {}^{8}\mathrm{Be}_{gs} + \alpha_3)$ and $E_x(^{12}\mathrm{C}^* \rightarrow {}^{8}\mathrm{Be}_{gs} + \alpha_4)$. The two excitation energies obtained in this way are shown plotted against each other in Fig. 6, for the data obtained at a beam energy of 28.0 MeV. It is noted that the data shown in Fig. 6 correspond to all $^{8}\mathrm{Be}_{gs}$ + not $^{8}\mathrm{Be}_{gs}$ events [the $E_x(^{9}\mathrm{Be}) \geqslant 3.5$ MeV gate discussed above was not applied]. The two horizontal and vertical loci seen in Fig. 6 correspond to the 7.65-MeV 0_2^+ and 9.64-MeV 3^- excited states in ^{12}C. These may be seen clearly in the upper and right panels, which are projections of the data onto the X and Y axes, respectively. The (red) boxes in the main panel indicate the gates used to select the two states.

The excitation energy spectra for the decay of ^{16}O to $^{12}\mathrm{C}^*$ [7.65 MeV] + α, obtained from the $^{13}\mathrm{C}(^{4}\mathrm{He}, ^{12}\mathrm{C}^*\ \alpha)n$ reaction, are shown in Fig. 7. In Fig. 7(a) all $^{8}\mathrm{Be}_{gs}$ + not $^{8}\mathrm{Be}_{gs}$ events proceeding via the 7.65-MeV 0_2^+ state in ^{12}C are shown, whereas in Fig. 7(b) the $E_x(^{9}\mathrm{Be}) \geqslant 3.5$ MeV gate (see above) are applied. The data shown correspond to all three beam energies added together. In both Figs. 7(a) and 7(b) the (blue) dot-dashed line indicates the experimental detection efficiency, for which the peak value is given.

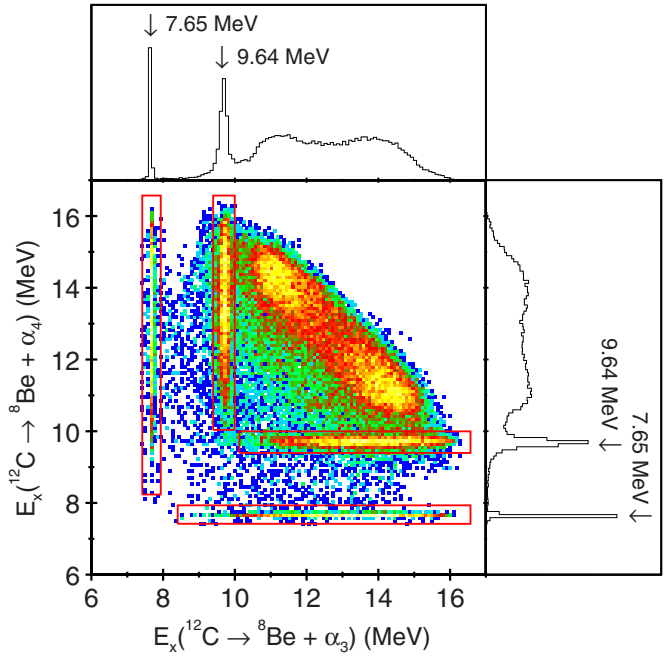

FIG. 6. Excitation energy in ^{12}C obtained from $E_{\mathrm{decay}}(^{8}\mathrm{Be}_{gs} + \alpha_3)$ against that obtained from $E_{\mathrm{decay}}(^{8}\mathrm{Be}_{gs} + \alpha_4)$, for $^{8}\mathrm{Be}_{gs}$ + not $^{8}\mathrm{Be}_{gs}$ events. The (red) boxes in the main panel indicate the windows used to select the 7.65- and 9.64-MeV states. In the upper and right panels the X and Y projections of the data are shown. The beam energy was 28.0 MeV.

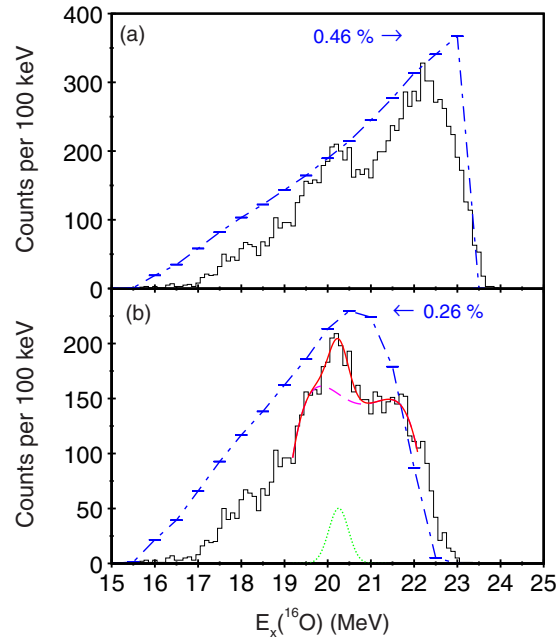

FIG. 7. Excitation energy for the $^{12}\mathrm{C}^*$ [7.65 MeV] + α decay of ^{16}O from (a) all events in the present data and (b) events with $E_x(^{9}\mathrm{Be}) \geqslant 3.5$ MeV. The (blue) dot-dashed lines represent the detection efficiency profiles, for which the peak values are given. (b) The results of a Gaussian peak fit are shown (see text).

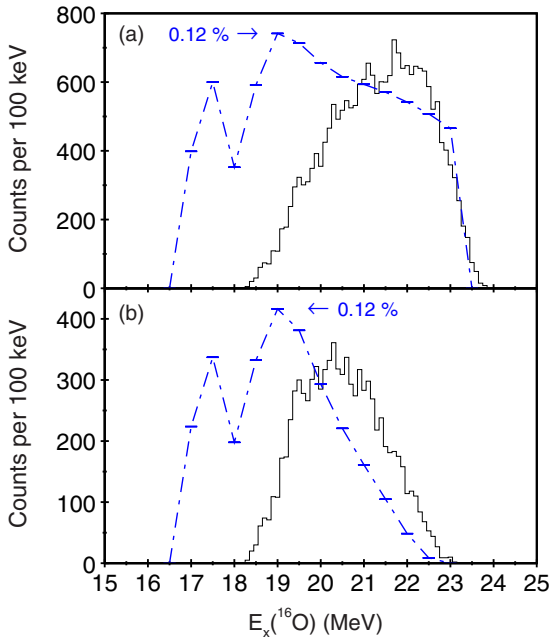

FIG. 8. Excitation energy for the $^{12}C^*$ [9.64 MeV] + α decay of ^{16}O from (a) all events in the present data and (b) events with $E_x(^9Be) \geqslant 3.5$ MeV. The (blue) dot-dashed lines represent the detection efficiency profiles, for which the peak values are given.

In Fig. 8 the ^{16}O excitation energy spectra obtained from the $^{13}C(^4He,^{12}C^*$ [9.64 MeV] $\alpha)n$ reaction, for all three beam energies added together, are shown. All events decaying via the ^{12}C 9.64-MeV 3^- state are shown in Fig. 8(a), and the subset for which $E_x(^9Be) \geqslant 3.5$ MeV is shown in Fig. 8(b). In Figs. 8(a) and 8(b) the experimental detection efficiency is indicated by the (blue) dot-dashed line, and the maximum value given. The dip in both efficiency profiles at $E_x(^{16}O) =$ 18 MeV arises from gating on the $E_x(^{12}C^* \rightarrow {}^8Be_{gs} + \alpha_3)$ against $E_x(^{12}C^* \rightarrow {}^8Be_{gs} + \alpha_4)$ spectrum shown in Fig. 6. The horizontal and vertical windows applied to the data to select the 9.64-MeV state must not cross, because in such a crossing region the ambiguity as to whether it was α_3 or α_4 that came from the $^{12}C^* \rightarrow {}^8Be_{gs} + \alpha$ decay would remain. Hence events in which both $E_x(^{12}C^* \rightarrow {}^8Be_{gs} + \alpha_3) = 9.64$ MeV and $E_x(^{12}C^* \rightarrow {}^8Be_{gs} + \alpha_4) = 9.64$ MeV are not selected, leading to the reduction in efficiency seen in Figs. 8(a) and 8(b).

IV. DISCUSSION

In the E_{tot} spectrum shown in Fig. 1, two distinct peaks, labeled $Q_{5g}(^{13}C)$ and $Q_{4g}(^{12}C)$, can be observed. As noted in Sec. III, these correspond to the $^{13}C(^4He,4\alpha)n$ and $^{12}C(^4He,4\alpha)$ channels, respectively. The yield in the $Q_{4g}(^{12}C)$ peak is ∼24% of that observed in the $Q_{5g}(^{13}C)$ peak, a much higher value than would be expected based on the nominal ∼1% ^{12}C present in the target. It should be noted, however, that the data presented in Fig. 1 correspond to the last beam energy (28.0 MeV) measured in the experiment. For the first beam energy (27.5 MeV), the $Q_{4g}(^{12}C)$ yield is ∼11% of that in the $Q_{5g}(^{13}C)$ peak, and for the 27.0 MeV data (taken between

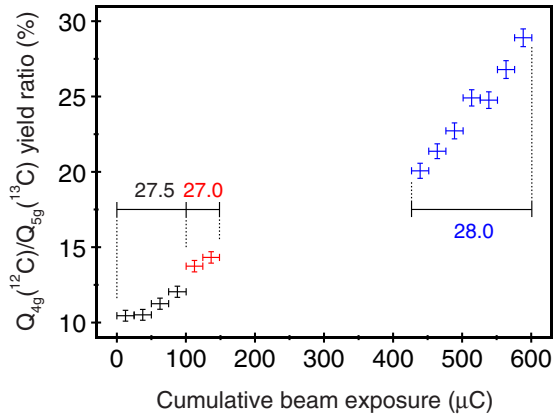

FIG. 9. Total energy spectrum (Fig. 1) $Q_{4g}(^{12}C)$ to $Q_{5g}(^{13}C)$ yield ratio as a function of cumulative beam exposure. The beam energies of 27.0 (red points), 27.5 (black points), and 28.0 MeV (blue points), at which the data points were obtained, are noted.

the 27.5 and 28.0 MeV beam energies) the ratio is 14%. The ratio of $Q_{4g}(^{12}C)$ to $Q_{5g}(^{13}C)$ yield is shown in Fig. 9, plotted against the cumulative beam exposure of the experiment. The data were analyzed in blocks of approximately 25 μC width (represented by the horizontal error bars). The vertical error bars were obtained from the statistical uncertainties on the peak yields. The cumulative beam exposure range of ∼150–425 μC, where no data points are plotted, corresponds to the 22.0-MeV beam measurements. At this energy no appreciable yield was observed in the $^{13}C(^4He,4\alpha)n$ channel. Whereas some variation in the $Q_{4g}(^{12}C)$ to $Q_{5g}(^{13}C)$ ratio would be expected due to the energy dependence of the $^{13}C(^4He,4\alpha)n$ and $^{12}C(^4He,4\alpha)$ cross sections, it is clear in Fig. 9 that there is a significant increase in the ratio (from ∼11% to 29%), not only as a general function of cumulative beam exposure (and hence time into the experiment), but also within individual beam energy measurements. This can be most clearly seen in the 28.0-MeV data (blue points), where the ratio increases from ∼20% to 29.5%. As these points correspond to a single beam energy, the increase in ratio cannot be the result of a change in either the $^{13}C(^4He,4\alpha)n$ or $^{12}C(^4He,4\alpha)$ cross section and must result from a change in the target composition. Figure 9 therefore provides clear evidence for significant carbon buildup on the target during the experiment, leading to the increase in $Q_{4g}(^{12}C)$ to $Q_{5g}(^{13}C)$ ratio observed. This hypothesis is supported by measurements of the $^{12}C(^4He,^8Be)^8Be$, $^{12}C(^4He,^{12}C^*$ [7.65 MeV, 0_2^+])α, and $^{12}C(^4He,^{12}C^*$ [9.64 MeV, 3^-])α excitation functions, which were made during the same experimental campaign at Notre Dame [21]. These data were obtained from two different ^{12}C targets (denoted $^{12}C_1$ and $^{12}C_2$). Each was measured before and after exposure to the beam, to allow the increase in thickness arising from carbon deposition to be determined. Target $^{12}C_1$ was measured to be ∼46 (53) $\mu g/cm^2$ before (after) exposure to the beam, indicating carbon buildup of 7 $\mu g/cm^2$. For target $^{12}C_2$, the thickness increased from ∼40 to 51 $\mu g/cm^2$, a buildup of 11 $\mu g/cm^2$. Because the present data were taken under the same experimental conditions (the same vacuum chamber and pumping system), and the mean beam

TABLE I. Centroid energies, widths (FWHM), and cross - sections (σ) for the peaks observed in the $^{8}Be_{gs} + {}^{8}Be_{gs}$ and $^{12}C^{*}$ [7.65 MeV] + α decay of ^{16}O, obtained for events with $E_x(^{9}Be) \geqslant 3.5$ MeV. The uncertainties are discussed in the text.

Channel	Centroid (MeV)	FWHM (keV)	σ (μb)
$^{8}Be_{gs} + {}^{8}Be_{gs}$	17.3 ± 0.2	199 ± 54	11.4 ± 2.8
$^{8}Be_{gs} + {}^{8}Be_{gs}$	18.0 ± 0.2	398 ± 91	14.1 ± 4.1
$^{8}Be_{gs} + {}^{8}Be_{gs}$	(18.9 ± 0.2)	(418 ± 27)	(17.9 ± 4.3)
$^{8}Be_{gs} + {}^{8}Be_{gs}$	19.4 ± 0.2	344 ± 4	104.0 ± 14.0
$^{12}C^{*}$ [7.65 MeV] + α	20.2 ± 0.2	520 ± 53	99.1 ± 23.6
$^{8}Be_{gs} + {}^{8}Be_{gs}$	21.0 ± 0.2	261 ± 47	22.3 ± 5.9

currents were similar for all three targets (4.9 nA for target $^{12}C_1$, 5.7 nA for target $^{12}C_2$, and 6.2 nA for the ^{13}C target), it is not unreasonable to expect a similar level of carbon buildup on the ^{13}C foil. Scaling for the different total beam exposures for the three target measurements (1009, 783, and 600 μC for targets $^{12}C_1$, $^{12}C_2$, and ^{13}C, respectively) suggests a total of 4.2–8.4 μg/cm^2 carbon deposition on the ^{13}C target. If it is assumed that the factor of 2.8 increase (from 10.5% to 29.5%) in $Q_{4g}(^{12}C)$ to $Q_{5g}(^{13}C)$ ratio observed in Fig. 9 arises solely from carbon buildup, then the initial ^{12}C thickness would be 2.3–4.4 μg/cm^2. This corresponds to ~5–10% of the nominal 45 μg/cm^2 ^{13}C target thickness, somewhat higher than the 1% ^{12}C expected from the quoted carbon ^{13}C enrichment.

The excitation energy spectrum for the $^{8}Be_{gs} + {}^{8}Be_{gs}$ decay of ^{16}O, obtained after the $E_x(^{9}Be) \geqslant 3.5$ MeV gate had been applied, can be seen in Fig. 5(b) [and with an expanded Y scale in Fig. 5(c)]. One strong peak can be observed, at $E_x = 19.4$ MeV, as can a number of weaker features. The spectrum was fitted with a series of Gaussian peak shapes above a smoothly varying background. The dotted (green) lines in Figs. 5(b) and 5(c) show the individual fitted peaks, the dashed (magenta) lines the background, and the smooth (red) lines the overall fit. The resulting centroids and widths (FWHM) obtained for four of the features observed in the spectrum are listed in Table I, as is the energy of one additional peak, which appears to give rise to a shoulder observed at 18.9 MeV. The uncertainties quoted for the centroids reflect a 200-keV systematic uncertainty in the peak energies, typical of that normally seen in breakup reactions such as those studied here. In all cases this systematic error dominates the statistical uncertainty of the fit. For the widths the uncertainties quoted are those obtained from the peak fitting routine only, and they reflect the statistical accuracy of the fit, for which the χ^2 per degree of freedom is 2.0.

The ^{16}O excitation energy spectra shown in Fig. 5 correspond to all three beam energies added together. To investigate the nature of the peaks observed in Figs. 5(b) and 5(c), the E_x spectra obtained at the three different beam energies are shown individually in Fig. 10. The data corresponding to beam energies of 27.0, 27.5, and 28.0 MeV are shown in Figs. 10(a), 10(c), and 10(e), and again, with expanded Y scales, in Figs. 10(b), 10(d), and 10(f), respectively. The E_x spectra were fitted with a number of Gaussian peak shapes

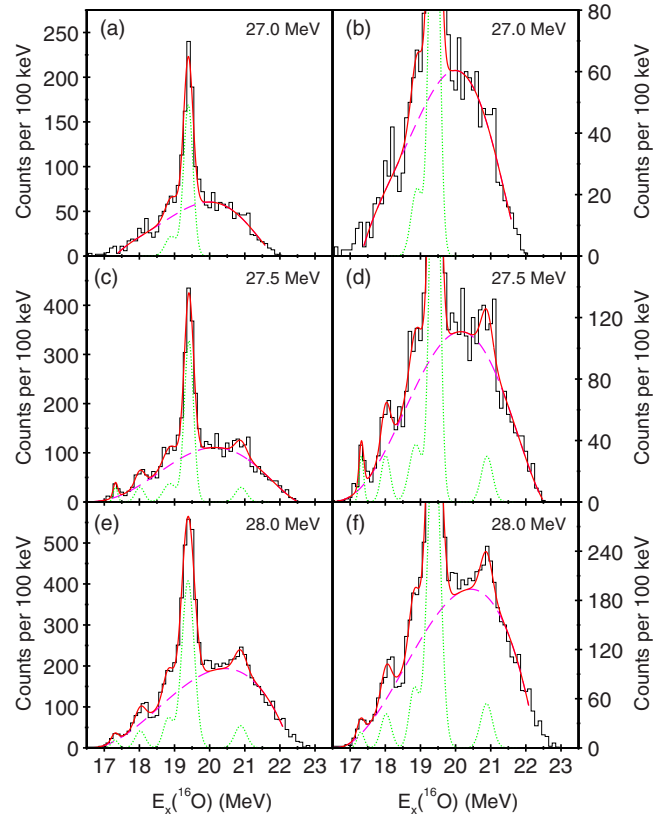

FIG. 10. Excitation energy for the $^{8}Be_{gs} + {}^{8}Be_{gs}$ decay of ^{16}O, at beam energies of (a, b) 27.0, (c, d) 27.5, and (e, f) 28.0 MeV. In (a), (c), and (e) the full spectra are shown, whereas in (b), (d), and (f) the Y scale has been expanded. In all panels the results of a Gaussian peak fit are shown (see text).

above a smoothly varying background, with the individual fitted peaks shown by the dotted (green) lines, the background by the dashed (magenta) lines, and the overall fit by the smooth (red) lines. Although there is perhaps some evidence for a peak at $E_x \sim 18.1$ MeV in the 27.0-MeV beam energy data [Figs. 10(a) and 10(b)], the limited statistics mean that a reliable fit can only be obtained when two peaks are included. These are the shoulder at 18.9 MeV and the strong peak at 19.4 MeV. In the case of both the 27.5-MeV [Figs. 10(c) and 10(d)] and 28.0-MeV [Figs. 10(e) and 10(f)] beam energy data, all five of the peaks seen in Figs. 5(b) and 5(c) (at $E_x = 17.3$, 18.0, 18.9, 19.4, and 21.0 MeV) can be observed and were fitted. The average variation in peak centroid across all of the fits is 30 keV. For the width, the variation is 70 keV. This observation, of the peaks at more than one beam energy, suggests that they do not correspond to statistical fluctuations in the data, but instead to states in ^{16}O, at these particular excitation energies.

The energy and width of the one peak for which a reliable fit could be obtained for the $^{13}C(^{4}He,{}^{12}C^{*}$ [7.65 MeV] $\alpha)n$ reaction [shown in Fig. 7(b)] is given in Table I. No reliable fit (of a Gaussian peak shape above a smoothly varying background) was obtained for the $^{13}C(^{4}He,{}^{12}C^{*}$ [9.64 MeV] $\alpha)n$ decay channel, shown in Fig. 8(b).

The cross sections for the peaks observed in the ^{16}O excitation energy spectra, for decays via the ^{13}C(^{4}He,^{8}Be$_{gs}$ ^{8}Be$_{gs}$)n and ^{13}C(^{4}He,^{12}C* [7.65 MeV] α)n channels, are listed in Table I. These values were determined from the yields obtained from the Gaussian peak fitting discussed above. At each beam energy the yields in the peaks were scaled by the beam exposure, the ^{13}C target thickness, and the experimental detection efficiency at the excitation energy of the peak centroids. The detection efficiencies were obtained from Monte Carlo simulations of the reactions and detector setup. In these simulations random number generators that reproduced the experimental center of mass (c.m.) angular distributions for the initial ^{13}C(^{4}He,^{16}O*)n reaction were used. These were obtained by studying the c.m. scattering angle (denoted θ^{*}) of the recoiling neutron. At each beam energy the full (0°–180°) c.m. angular range was observed. Because of statistical limitations, only one θ^{*} random number generator was produced per beam energy, for each of the ^{8}Be$_{gs}$ + ^{8}Be$_{gs}$ and ^{12}C* [7.65 MeV] + α decay channels (a separate θ^{*} generator was not used for each individual state). The sequential decay of the excited ^{16}O* to ^{8}Be$_{gs}$ + ^{8}Be$_{gs}$ and ^{12}C* [7.65 MeV] + α was simulated with an isotropic distribution. The uncertainties were calculated at each energy from the statistical errors on the fitted yield for each of the peaks, and from an estimated 20% systematic uncertainty in the ^{13}C target thickness. An additional uncertainty also arises from the use of a single θ^{*} random number generator at each beam energy, as opposed to an individual distribution for every peak. An estimate of the uncertainty this produces in the Monte Carlo predicted detection efficiency was obtained by repeating the cross-section calculations, using efficiencies obtained with isotropic θ^{*} distributions (rather than those measured experimentally). This analysis indicates a cross-section variation of up to 10%, and this value was included in the calculation of the overall error in the cross-section values. As no significant variation in cross section with beam energy was observed, the values listed in Table I represent weighted averages for the three different beam energies used in the experiment.

A comparison of the ^{8}Be$_{gs}$ + ^{8}Be$_{gs}$ breakup excitation energy spectrum [solid (black) line] with the ^{12}C(^{4}He,^{8}Be)^{8}Be 90° yield excitation function of Curtis *et al.* [21] [dotted (red) line] can be seen in Fig. 11(a). All of the peaks observed in the breakup spectrum (and listed in Table I) appear to correspond to features in the excitation function. The weakly populated peak seen at 17.3 ± 0.2 MeV in the present work appears close to the energy of both the 17.15-MeV 2^{+} resonance reported by Chevallier *et al.* [1] and the 17.5-MeV 2^{+} state observed in the ^{8}Be + ^{8}Be breakup of ^{16}O by Freer *et al.* [18]. In the later excitation function measurement of Curtis *et al.* [21] it was suggested that a narrow 2^{+} resonance exists at 17.10 MeV, interfering with a broad structure appearing between 16.5 and 17.5 MeV. There is only one state known to decay to the ^{8}Be + ^{8}Be channel listed in the current mass 16 compilation [3], within the ±200 keV uncertainty range in the centroid energy of the 17.3-MeV peak. This is the (17.197 ± 0.017)-MeV, (160 ± 60)-keV-wide, 2^{+} state [listed with an energy of 17.17 MeV (Table 16.12) in an earlier compilation [34]]. The same centroid of 17.17 MeV

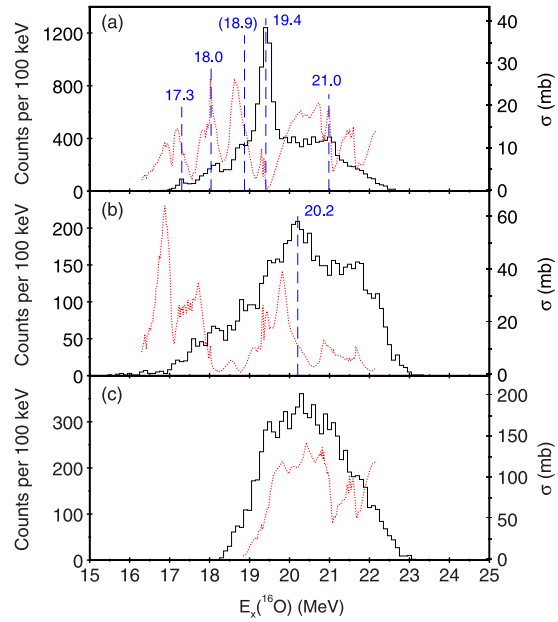

FIG. 11. Excitation energy obtained from the ^{13}C(^{4}He,4α)n breakup reaction [solid (black) lines and left-hand Y scale] and ^{12}C(^{4}He,4α) excitation functions of Curtis *et al.* [21] [dotted (red) lines and right-hand Y scale), for the (a) ^{8}Be$_{gs}$ + ^{8}Be$_{gs}$, (b) ^{12}C* [7.65 MeV] + α, and (c) ^{12}C* [9.64 MeV] + α decay of ^{16}O. The vertical (blue) dashed lines indicate the energies (in MeV) of the fitted peaks and features (see text).

is also given by Ames [17], who observed decay to the ^{12}C* [7.65 MeV] + α channel from a weak state at this energy, with a width of ∼150 keV. Ames suggested that this state could correspond to the ∼200-keV-wide 2^{+} resonance observed in the ^{12}C(^{4}He,^{8}Be)^{8}Be channel. Taken together, this suggests that the (17.3 ± 0.2)-MeV peak seen in the present work is a candidate for a 2^{+} state, although due to the poor coverage and statistics in this region, this assignment must remain tentative.

In the mass 16 compilation [3], there is only one state listed within the 200-keV excitation energy uncertainty range of the (18.0 ± 0.2)-MeV peak observed in the current work that is known to decay to the ^{8}Be channel. This 4^{+} state, at 18.016 ± 0.001 MeV, was found by Ames [17] to also decay to the ^{12}C* [7.65 MeV] + α channel and was suggested to be an excited core state. In the Curtis *et al.* [21] excitation function, a 4^{+} resonance was also identified at 18.03 MeV, and a (2^{+}, 4^{+}) state has been seen at 18.0 MeV in the ^{12}C(^{16}O,4α)^{12}C breakup reaction [18]. Similarly, Chevallier *et al.* [1] observed a 4^{+} resonance at 18.05 MeV in the ^{8}Be$_{gs}$ + ^{8}Be$_{gs}$ channel and also found a resonance at the same energy in the ^{15}N + p system. This suggests that the (18.0 ± 0.2)-MeV peak observed in the current breakup work may correspond to a 4^{+} state at this energy in ^{16}O. There is also some evidence for a shoulder in the present breakup spectrum at E_x = 18.9 ± 0.2 MeV, which may correspond to the broad (L = 4) feature seen at around 18.6 MeV in the Curtis *et al.* [21] excitation function. Two broad states, that decay to the ^{8}Be channel, are listed in Ref. [3] in this region, at 18.6 and 18.785 ± 0.006 MeV, with widths and spin assignments of ∼300 keV and 4^{+}, and 260 ± 20 keV and 4^{+}, respectively. It is possible that the shoulder seen at

$E_x = 18.9 \pm 0.2$ MeV in Fig. 11(a) might correspond to an unresolved, weak population of these two states.

The strongest peak in the current breakup work, at 19.4 ± 0.2 MeV, appears at an energy close to the 19.3-MeV 4^+ state seen in the Freer *et al.* [18] data, and the only state listed in the 19.2–19.6 MeV region in the mass 16 compilation [3] that decays to ^{8}Be, the (6^+) state at 19.319 MeV (observed by Ames [17] to also decay to the $\alpha + {}^{12}$C channel). The (19.4 ± 0.2)-MeV peak is also close to the 19.35-MeV 6^+ resonance reported by Chevallier *et al.* [1]. This resonance was found in the later ^{12}C(^{4}He,^{8}Be)^{8}Be excitation function measurement of Curtis *et al.* [21], however, to be a double peak at $E_x = 19.29$ and 19.36 MeV. A phase shift analysis of this double peak suggested it arose from the interference between the background and a single, narrow, $J^\pi = 2^+$ or 4^+ resonance at 19.3 MeV. The observation of a peak in this excitation energy region in all four channels [the current ^{13}C(^{4}He,^{8}Be$_{gs}$ ^{8}Be$_{gs}$)n breakup reaction, the ^{12}C(^{16}O,^{8}Be$_{gs}$ ^{8}Be$_{gs}$)^{12}C breakup reaction [18], the ^{12}C(^{4}He,^{8}Be$_{gs}$)^{8}Be$_{gs}$ excitation function [21], and in α decay [17]] suggests that a state does exist in ^{16}O at this energy, with the breakup study of Freer *et al.* [18] indicating a spin and parity of 4^+. There is also some evidence for a peak in the present measurement at $E_x = 21.0 \pm 0.2$ MeV, the same energy as a narrow 4^+ or 6^+ feature in the Curtis *et al.* [21] excitation function (at $E_x = 21.0$ MeV). The observation of structure in both spectra supports the hypothesis that there may be a state in ^{16}O at this energy, and it is possible that this state corresponds to the 6^+ state seen at 21.4 MeV in the Freer *et al.* work [18], which is in turn supported by the observation of a 6^+ state at 21.2 MeV in a study of the ^{12}C(^{12}C,^{8}Be$_{gs}$ ^{8}Be$_{gs}$)^{8}Be$_{gs}$ reaction [19].

In Fig. 11(b) the excitation energy spectrum for the decay of ^{16}O to ^{12}C* [7.65 MeV] + α [solid (black) line] is shown, along with the Curtis *et al.* [21] ^{12}C(^{4}He,^{12}C* [7.65 MeV])α 90° yield excitation function [dotted (red) line]. A similar comparison is made in Fig. 11(c) for decay via the 9.64-MeV 3^- state in ^{12}C. The peak observed at 20.2 ± 0.2 MeV in the ^{12}C* [7.65 MeV] + α breakup channel shown in Fig. 11(b) appears to have no counterpart in the excitation function, suggesting it either does not correspond to a state in ^{16}O, or arises from the decay of a state in ^{16}O that is not populated in the ^{12}C(^{4}He,^{12}C* [7.65 MeV])α reaction. No firm conclusions can be drawn from this comparison, however, as the features of the breakup spectra are both weak and poorly resolved.

The most striking feature of the three ^{16}O excitation energy spectra shown in Fig. 11 is the strength of the peak observed at 19.4 ± 0.2 MeV in the ^{13}C(^{4}He,^{8}Be ^{8}Be)n channel. This state is much more strongly populated (by a factor of 5–9) than the other peaks seen in the ^{8}Be + ^{8}Be breakup of ^{16}O [solid (black) line in Fig. 11(a), and listed in Table I]. This is in contrast to the ^{12}C(^{4}He,^{8}Be)^{8}Be 90° excitation function [dotted (red) line in Fig. 11(a)], in which the $J^\pi = 2^+$ or 4^+ resonance at 19.3 MeV (observed as a double peak at 19.29 and 19.36 MeV) is much weaker than the surrounding features. The ^{12}C(^{4}He,^{8}Be)^{8}Be channel is a resonance reaction, with a cross section given by

$$\sigma \propto \frac{(2J+1)\Gamma_\alpha \Gamma_{^{8}\mathrm{Be}}}{(E - E_x)^2 + \Gamma_{\mathrm{tot}}^2/4},$$

where Γ_α is the ^{12}C + ^{4}He entrance channel partial width, $\Gamma_{^{8}\mathrm{Be}}$ the ^{8}Be + ^{8}Be exit channel partial width, and Γ_{tot} the full width of the resonance. This cross section is dependent on the spin of the resonance, J, indicating the low spin ($J^\pi = 2^+$ or 4^+) of the 19.3-MeV resonance will cause a relatively low cross section for population via the ^{12}C(^{4}He,^{8}Be)^{8}Be resonance reaction. In the case of the ^{13}C(^{4}He,^{8}Be ^{8}Be)n reaction, the ^{13}C + ^{4}He entrance channel can populate a variety of spin states in ^{17}O, which will in turn neutron decay, to populate the states observed in ^{16}O. Because the neutron would be expected to carry away low spin, the ^{13}C(^{4}He,^{16}O*)n reaction will preferentially populate low spin states in ^{16}O. Hence, for a low spin state, the cross section will be small in the ^{12}C(^{4}He,^{8}Be)^{8}Be resonance reaction, and large in the ^{13}C(^{4}He,^{8}Be ^{8}Be)n breakup channel, as seen with the (19.4 ± 0.2)-MeV peak in Fig. 11(a). This adds support to the $J^\pi = 2^+$ or 4^+ assignment made in Ref. [21].

V. SUMMARY

The ^{13}C(^{4}He,^{8}Be ^{8}Be)n and ^{13}C(^{4}He,^{12}C* α)n reactions have been studied at beam energies of 27.0, 27.5, and 28.0 MeV. A comparison with previous measurements of both the ^{12}C(^{4}He,^{8}Be)^{8}Be excitation function and ^{12}C(^{16}O,4α)^{12}C breakup channel suggests a 4^+ state may exist in ^{16}O at an excitation energy of 18.0 ± 0.2 MeV, with tentative evidence also being found for a 2^+ state at 17.3 ± 0.2 MeV and a 4^+ or 6^+ state at 21.0 ± 0.2 MeV. The strongest state observed in the current work, at 19.4 ± 0.2 MeV, appears to correspond to the 2^+ or 4^+ resonance seen at 19.3 MeV in a previous study of the ^{12}C(^{4}He,^{8}Be)^{8}Be excitation function [21], and the 4^+ state observed at 19.3 MeV in the breakup measurement of Freer *et al.* [18]. The relative cross sections expected for resonant and sequential breakup reactions also suggest the state is of low spin.

It is clear that much work still needs to be performed in order to clarify the situation regarding the four α-linear chain state in ^{16}O. Measurements in the excitation energy region suggested by the calculations of Ichikawa *et al.* [25] and Yao *et al.* [27], in which the rotational bandhead appears in the $E_x = 30$–38 MeV region, appear extremely challenging experimentally. However, a high resolution breakup measurement in the present 16–23 MeV range should be possible. A repeat of the ^{12}C(^{16}O,4α)^{12}C breakup study of Freer *et al.* [18] at high resolution would, for example, allow spin assignments to be made for the various structures of interest and allow a more detailed comparison with the ^{12}C(^{4}He,^{8}Be)^{8}Be excitation function measurements of Chevallier *et al.* [1] and Curtis *et al.* [21].

ACKNOWLEDGMENTS

The assistance of the staff at the University of Notre Dame FN Tandem facility is gratefully acknowledged. This work was funded by the United Kingdom Science and Technology Facilities Council and the United States National Science Foundation under Contract No. PHY08-22648. One of the authors (G.G.) would like to thank Professor Daniel Zajfman and Professor Yossi Nir of the Weizmann Institute for financial support.

[1] P. Chevallier, F. Scheibling, G. Goldring, I. Plesser, and M. W. Sachs, Phys. Rev. **160**, 827 (1967).
[2] H. Morinaga, Phys. Rev. **101**, 254 (1956).
[3] D. R. Tilley, H. R. Weller, and C. M. Cheves, Nucl. Phys. A **564**, 1 (1993).
[4] M. Freer, Rep. Prog. Phys. **70**, 2149 (2007).
[5] W. Bauhoff, H. Schultheis, and R. Schultheis, Phys. Rev. C **29**, 1046 (1984).
[6] S. Aberg, I. Ragnarsson, T. Bengtsson, and R. Sheline, Nucl. Phys. A **391**, 327 (1982).
[7] S. J. Krieger, Phys. Rev. Lett. **22**, 97 (1969).
[8] N. E. Reid, N. E. Davison, and J. P. Svenne, Phys. Rev. C **9**, 1882 (1974).
[9] B. Buck, C. B. Dover, and J. P. Vary, Phys. Rev. C **11**, 1803 (1975).
[10] J. D. Larson and R. H. Spear, Nucl. Phys. **56**, 497 (1964).
[11] J. Lowe, A. R. Poletti, and D. H. Wilkinson, Phys. Rev. **148**, 1045 (1966).
[12] Ph. Martin and T. R. Ophel, Nucl. Phys. A **194**, 491 (1972).
[13] D. R. James, J. L. Artz, M. B. Greenfield, and N. R. Fletcher, Nucl. Phys. A **227**, 349 (1974).
[14] F. Brochard, P. Chevallier, D. Disdier, V. Rauch, G. Rudolf, and F. Scheibling, Phys. Rev. C **13**, 967 (1976).
[15] A. D. Frawley, A. Roy, J. F. Mateja, and N. R. Fletcher, Nucl. Phys. A **363**, 280 (1981).
[16] S. J. Sanders, L. M. Martz, and P. D. Parker, Phys. Rev. C **20**, 1743 (1979).
[17] L. L. Ames, Phys. Rev. C **25**, 729 (1982).
[18] M. Freer, N. M. Clarke, N. Curtis, B. R. Fulton, S. J. Hall, M. J. Leddy, J. S. Pople, G. Tungate, R. P. Ward, P. M. Simmons, W. D. M. Rae, S. P. G. Chappell, S. P. Fox, C. D. Jones, D. L. Watson, G. J. Gyapong, S. M. Singer, W. N. Catford, and P. H. Regan, Phys. Rev. C **51**, 1682 (1995).
[19] M. Freer, M. P. Nicoli, S. M. Singer, C. A. Bremner, S. P. G. Chappell, W. D. M. Rae, I. Boztosun, B. R. Fulton, D. L. Watson, B. J. Greenhalgh, G. K. Dillon, R. L. Cowin, and D. C. Weisser, Phys. Rev. C **70**, 064311 (2004).
[20] A. Soylu, M. Freer, N. I. Ashwood, N. Curtis, T. Munoz-Britton, S. Spencer, C. Wheldon, V. Ziman, S. Brown, J. S. Thomas, G. Wilson, and G. Goldring, Phys. Rev. C **86**, 057601 (2012).
[21] N. Curtis, S. Almaraz-Calderon, A. Aprahamian, N. I. Ashwood, M. Barr, B. Bucher, P. Copp, M. Couder, X. Fang, M. Freer, G. Goldring, F. Jung, S. R. Lesher, W. Lu, J. D. Malcolm, A. Roberts, W. P. Tan, C. Wheldon, and V. A. Ziman, Phys. Rev. C **88**, 064309 (2013).
[22] A. C. Merchant and W. D. M. Rae, Nucl. Phys. A **549**, 431 (1992).
[23] A. C. Merchant and W. D. M. Rae, Z. Phys. A **349**, 243 (1994).
[24] A. C. Merchant and W. D. M. Rae, Phys. Rev. C **53**, 775 (1996).
[25] T. Ichikawa, J. A. Maruhn, N. Itagaki, and S. Ohkubo, Phys. Rev. Lett. **107**, 112501 (2011).
[26] L. Lang and Z. Peng-Wei, Chin. Phys. C **36**, 818 (2012).
[27] J. M. Yao, N. Itagaki, and J. Meng, Phys. Rev. C **90**, 054307 (2014).
[28] A. Tohsaki, H. Horiuchi, P. Schuck, and G. Röpke, Phys. Rev. Lett. **87**, 192501 (2001).
[29] S. Ohkubo and Y. Hirabayashi, Phys. Lett. B **684**, 127 (2010).
[30] T. Suhara, Y. Funaki, B. Zhou, H. Horiuchi, and A. Tohsaki, Phys. Rev. Lett. **112**, 062501 (2014).
[31] N. Curtis, A. St. J. Murphy, M. J. Leddy, J. S. Pople, N. M. Clarke, M. Freer, B. R. Fulton, S. J. Hall, G. Tungate, R. P. Ward, S. M. Singer, W. N. Catford, G. J. Gyapong, R. A. Cunningham, J. S. Lilley, S. P. Chappell, S. P. Fox, C. D. Jones, D. L. Watson, P. M. Simmons, R. A. Hunt, A. C. Merchant, A. E. Smith, W. D. M. Rae, and J. Zhang, Nucl. Instrum. Methods Phys. Res. Sect. A **351**, 359 (1994).
[32] D. R. Tilley, J. H. Kelley, J. L. Godwin, D. J. Millener, J. E. Purcell, C. G. Sheu, and H. R. Weller, Nucl. Phys. A **745**, 155 (2004).
[33] M. Freer, Nucl. Instrum. Methods Phys. Res. Sect. A **383**, 463 (1996).
[34] F. Ajzenberg-Selove, Nucl. Phys. A **460**, 1 (1986).